Design and operation for ultra low noise take-off

Daniel Crichton[1], Elena de la Rosa Blanco[2] and Thomas R. Law[3]
Cambridge University Engineering Department, Cambridge, CB3 0DY, UK

and

James I. Hileman[4]
Massachusetts Institute of Technology, Cambridge, MA 02139

Meeting the Silent Aircraft Initiative (SAI) design goal during take-off drives the aircraft and engine design towards a multi-engine configuration with low specific thrust and high cruise altitude. These design choices enable the engine fan to operate at part-speed during take-off, significantly increasing the benefit of a variable area nozzle in relation to fan and jet source noise reduction. By optimizing the thrust and climb gradient for low jet noise during the entire take-off it is possible to reduce jet noise to the SAI target of 60 dBA. Using this approach overall aircraft noise meets the SAI target at the sideline location but is approximately 5dBA above the target at the flyover location. By considering turbomachinery and airframe noise sources when optimizing thrust and climb gradient it is possible to match the peak noise produced at all times during take-off giving an overall noise level of 62 dBA.

Nomenclature

<u>Latin</u>

A	=	area
D	=	drag
c_D	=	coefficient of drag
C_{FG}	=	thrust coefficient
FPR	=	fan stage pressure ratio
g	=	acceleration due to gravity
L	=	lift
m	=	mass
n_{eng}	=	number of engines
N	=	noise limit
M	=	Mach number
p	=	pressure
PR	=	pressure recovery
Q	=	capacity
T	=	temperature
T_N	=	net thrust
T_G	=	gross thrust
ToC	=	Top of Climb
U	=	corrected fan speed
V	=	Velocity

<u>Greek</u>

α	=	angle of attack
β	=	thrust vector angle
γ	=	ratio of specific heat capacities
η	=	fan efficiency
θ	=	climb angle
μ	=	coefficient of drag
φ	=	flow coefficient

<u>Subscripts</u>

0	=	stagnation conditions
ff	=	fan face
in	=	inlet (free stream to fan face)
jet	=	fully expanded jet
noz	=	nozzle
out	=	exhaust (fan exit to fully expanded including correction for core mixing)
p	=	polytropic
R	=	rotation
x	=	axial
∞	=	free stream

[1] PhD Student, Whittle Laboratory, Department of Engineering, Madingley Road, Cambridge, CB3 0DY, UK, AIAA Student Member

[2] Research Associate, Whittle Laboratory, Department of Engineering, Madingley Road, Cambridge, CB3 0DY, UK, AIAA Member

[3] PhD Student, Department of Engineering, Trumpington Road, Cambridge, CB2 1PZ, UK, AIAA Student Member

[4] Research Engineer, Gas Turbine Laboratory, Department of Aeronautics and Astronautics, Massachusetts Institute of Technology, Cambridge, MA 02139, AIAA Member

I. Introduction

This paper is part of a collection that document the final design and estimated noise footprint of the concept aircraft developed as part of the Silent Aircraft Initiative[1-6]. The aircraft, based on 2025 technology estimates and timeframes, has been designed against the aim of being imperceptible outside the airport boundary in an urban environment. This goal, significantly more challenging that the ACARE 2020 noise target[7] (see Fig. 1) was translated into a specific target noise level of 60 dBA. This value can be linked to both World Health Organization guidelines on community noise[8] and data on average traffic noise levels in a typical urban area[9]. An A-weighted decibel value was used as, unlike EPNdB or DNL values, it does not require prior knowledge of flight profiles or traffic patterns and is therefore easier to design against.

To meet the target during take-off requires not only reduction in both aircraft and engine noise sources but also optimization of the departure profile to deliver low noise. Traditionally, jet and fan noise are dominant at take-off and, whereas fan noise can be tackled through shielding[10] and extending duct lengths[11], jet noise represents a noise floor that must be considered at the start of the design process. This approach formed the basis of the initial engine design effort with take-off optimization for low jet noise at fixed jet area[12] feeding into the selection of fan pressure ratio and the preliminary fan design[13]. In this paper enhancements to this approach are presented with jet area being continually modified so that the fan can operate at an ideal location and the take-off optimization being extended to cover noise sources other than the jet.
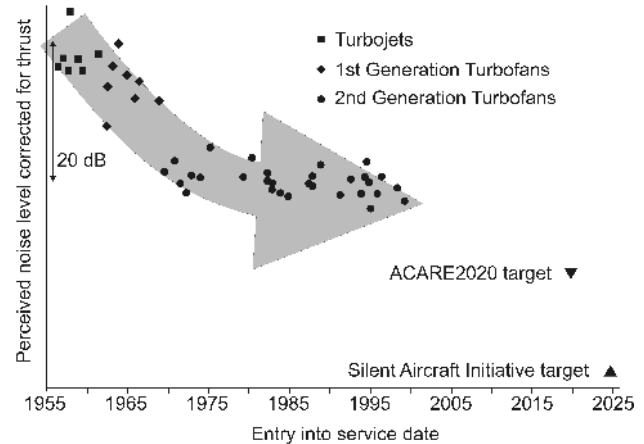

Figure 1. Reduction in thrust corrected aircraft noise level over time

II. Design for low noise

A. Airframe

The silent aircraft utilizes an all-lifting-body airframe where the fuselage provides lift and the aircraft lacks tail surfaces. The all-lifting-body airframe combines highly efficient airfoil profiles with a large lifting area to obtain both high efficiency at cruise and low stall speeds for low noise takeoff and landing operation. The silent aircraft design[14] differs significantly from other blended-wing-body designs[15] in that it utilizes aerodynamic shaping of the leading edge of the centerbody to achieve a 12% improvement in cruise aerodynamic efficiency, in terms of Mach times lift-to-drag ratio, while lowering the aircraft stall speed 28% below that typical of currently used aircraft. Gains in high-speed and low-speed performance were achieved simultaneously through optimization of the airfoil profiles and planform shape using a cost function that combined fuel burn with stall speed. The design process resulted in the use of leading edge aerodynamic shaping to provide lift that balances that created by the supercritical outer wing airfoil profiles without the need for canard or other lifting surfaces. The cruise altitude variation of 40,000 to 45,000 ft was defined early in the design process[16] as it yielded the lowest takeoff weight and therefore the lowest fuel consumption. The airframe centerbody provides shielding of forward radiating engine noise and ample room for acoustic liners to attenuate rearward propagating engine noise. To augment lift during takeoff and approach the airframe uses a deployable drooped leading edge and, like other tail-less configurations, lacks deployable flaps. Both of these lead to reduced airframe noise during takeoff and landing operations. Low speed aerodynamic data were estimated using the methods outlined in Ref 14 with the lift, drag, and moment coefficients for this design presented in Appendix B.

B. Engine

With the engine design presented in more detail in Ref 3, this section only summarizes the engine and presents some of the key features that enable an ultra low noise take-off. The final design consists of three engine clusters each of which has a primary engine and two auxiliary fans. These auxiliary fans are driven through a gearing arrangement by the low pressure turbine which also drives a similar fan which is conventionally located as part of the primary engine. To minimize jet temperature, the LPT exit flow is fully mixed with the bypass flow from the

primary fan, mixing with the flows from the auxiliary fans not being practical in the available space. The rotational speed of the fans is the same as the rotational speed of the LPT and the exhaust nozzle area can be modified to enable the fan to operate at a range of mass flow rates and pressure rises.

Whereas conventional aircraft in this SAI weight range (MTOW ~ 150,000kg) would have two engines, utilizing three engines has a significant noise benefit on take-off when trying to reduce noise outside of the airport boundary. For the SAI baseline airport the critical take-off condition is the engine out climb angle and, the higher the number of independent engines, the lower this angle. This reduces the thrust required and the resulting jet noise. Increasing the number of independent engines beyond three has reducing benefit and leads to increasing losses in the core and increased maintenance costs.

Although distributing the power from the LPT to different rotational axes will be a major technical challenge, the auxiliary engine design has several benefits. Rearward propagating noise can be reduced as, for the same airframe suction surface real-estate, the exhaust duct length to diameter ratio is increased. Forward propagating noise is also reduced as the nacelle exit is closer to the airframe surface improving shielding. Finally, even if auxiliary fans were not used, a speed reduction gearbox between LPT and fan would be required in order to keep LPT size and weight down at the same time as having a low tip speed fan.

For low take-off jet noise the engines need to deliver a high mass flow at a low velocity. This is achieved through increasing the nozzle area at take-off relative to the area at top of climb and cruise. Increasing nozzle area has several benefits. Firstly, as the design fan pressure rise is reduced and bypass ratio increases the fan working lines at cruise and take-off diverge. Cruise efficiency must be maximized and this leads to reducing stall margin at take-off. For the same thrust, opening the nozzle moves the fan operating point to a higher mass flow and lower pressure rise. At high speed the amount the nozzle area can be increased is limited by fan choking with the margin between stall and choke very small at top of climb design speed. Therefore to make full use of a variable area nozzle to reduce jet noise the fan needs to operate at part speed during take-off where larger nozzle increases can occur before the fan chokes. This is achieved in the SAI design by cruising at high altitude and utilizing a large lightly loaded wing (see above). The first increases the thrust available at take-off by increasing fan diameter and the second reduces the thrust required as take-off performance is improved. Operating at part-speed during take-off has the further advantage of reducing blade speed and fan source noise without requiring increased fan loading at top of climb.

III. Take-off optimization

To make a sizeable reduction in radiated jet noise the jet velocity must be reduced which leads to an increase in jet area for a fixed thrust. This requirement, for conventional turbofan engines, directly leads to an increase in engine bypass ratio and a reduction in fan pressure ratio as core pressure rise and turbine exit temperature cannot be reduced due to the impact on thermal efficiency. This will lead to increased propulsive efficiency at the expense of additional weight and installation drag losses. As seen in previous work[13, 17], in order to meet the target noise level, the required reduction in fan pressure ratio is to a value well below the optimum for today's technology and installations. Therefore any increase in jet area needs to be minimized and optimization of the departure profile is one way of achieving this. The approach taken is to split the take-off into three phases; acceleration, roll and climb. During the acceleration phase, the thrust is maximized without exceeding the target noise level outside of the airport. This continues until the specified roll velocity, V_R, is met. At this point the aircraft roll commences whilst maintaining acceleration again without exceeding the specified noise level. Once lift exceeds weight the aircraft is airborne and the climb phase starts. Here the aircraft velocity is kept constant and climb angle maximized. Increasing climb angle requires increased thrust and this is limited by the noise target. Once the aircraft is well clear of the airport the take-off profile is evaluated against take-off requirements including minimum climb angles, field length requirements and accelerate-stop distances[18, 19]. If any requirement is not met either the aircraft parameters are modified or the noise target relaxed and the take-off repeated. This continues until all take-off requirements are just met giving minimum take-off noise for a given aircraft, airport and conditions.

A. Baseline airport and conditions
A baseline airport was used to design the concept aircraft for and evaluate performance against. With London airports in particular subjected to significant noise constraints the baseline airport was chosen to cover the most restrictive of London conditions (approximately at ISA sea level). As such, runway length was set to 10,000 feet which is short by international 'hub' standards but is a common length for regional 'spoke' airports. ICAO certification distances[20] of 2000m approach (from threshold), 450m sideline and 6500m flyover (from brakes off) do
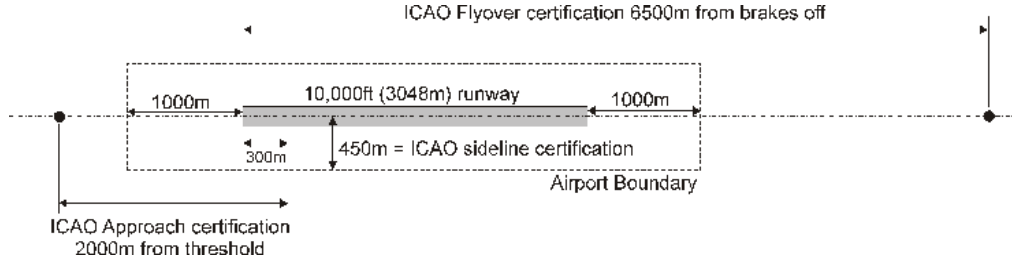
Figure 2. Baseline airport used to design aircraft against

not match most airport boundaries with the flyover position in particular being well outside most airports. After examining a range of airport boundaries the baseline values were set to 1000m from the start and end of the runway and 450m sideline as illustrated in Fig. 2. The hotter the conditions the lower the air density and the greater the jet velocity required for a given thrust. Therefore as jet temperature, which is linked to atmospheric temperature, increases it becomes harder to meet a jet noise target for a given jet area. Baseline airport temperature therefore needs to be specified at a high value so as to cover the majority of airport operation hours. Allowing 1% of 0600 to 2300 operating time to be non-silent[21], the required maximum 'silent' operating temperature was set to ISA+12°K.

B. Aircraft Modeling

Figure 3 shows the aircraft used during the take-off modeling in which W is zero in the air and θ is zero on the

Figure 3. Aircraft model for take-off optimization

ground. Drooped leading edge devices were deployed for take-off to increase achievable angle of attack but trailing edge brushes, used to reduce airframe noise on approach, are not deployed. As the purpose of the work was to look at resultant noise rather than aircraft stability, the thrust vector angle, β, was set to give zero moment at all time-steps, even when pitch angle was changing.
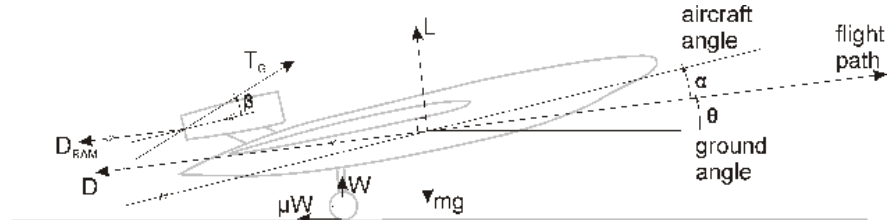
C. Preliminary optimization for fixed jet area and temperature

Before looking at engine performance in any detail, preliminary take-off optimization was performed with the engine modeled as just a jet of specified area and temperature. At each time step the jet velocity was maximized without the specified jet noise level being exceeded. The approach used was based on that in Ref 12 and is documented in detail in Ref 22.

For the baseline airport, engine out climb angle was found to be the critical requirement in ensuring a successful take-off with accelerate-stop and take-off distance requirements only becoming important for aircraft requiring high take-off speed (V_R above 80m/s). This is illustrated in Fig. 4 with take-off 1.6 km after brakes off followed by a steep climb whilst the aircraft is still within the airport boundary. This climb angle is limited by noise along the sideline. As the end of the airport boundary is approached, 4048m after brakes off, climb angle must reduce significantly so as not to exceed the noise limit directly below the aircraft at the flyover position. The climb angle at this point must not be less than the engine out minimum. Once beyond the airport boundary the

Figure 4. Example optimised departure with climb angle at flyover critical

distance from aircraft to ground gradually increases and the climb angle can therefore gradually be increased without the noise limit being exceeded.
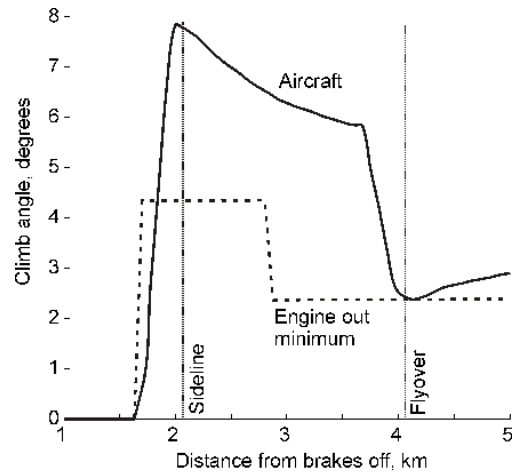
This minimum aircraft climb angle for normal operation, θ_{min}, can be calculated using Eq.(1) based on the regulated climb angle after engine out, θ^*, the number of independent engines, n_{eng}, and the lift to drag ratio before and after engine out. The 1.11 factor is a thrust increase allowance for an Automatic Takeoff Thrust Control System

(ATTCS)[18, 19]. Appendix A presents the approach taken for estimating the change in L/D following engine out for a tailless all-lifting-body aircraft.

$$\theta_{\min} \approx \sin^{-1}\left(\frac{1}{1.11}\frac{n_{eng}}{n_{eng}-1}\left(\left.\frac{1}{L/D}\right|_{after}+\sin\theta^*\right)-\left.\frac{1}{L/D}\right|_{before}\right) \tag{1}$$

Regression analysis was performed for a range of aircraft parameters and noise targets. Three to the power six optimizations were carried out with the following parameters varied:

- m   = 100,000kg   200,000kg   300,000kg
- L/D   = 16   22   28
- V_R = 50 m/s   60 m/s   70 m/s
- $T_{jet} - T_\infty$ = 25K   50K   75K
- n_{eng} = 2   3   4
- Noise target   = 54dBA   64dBA   74dBA

Wing area was modified to keep m * A_{wing} * V_R^2 constant so as to maintain similar angles of attack for all combinations. Equation (2) is the result of this analysis. The equation, only suitable for the SAI baseline airport and conditions, links aircraft parameters during take-off to the jet noise target that can be achieved. N_{jet} is the aircraft jet noise limit outside of the airport boundary, m is the aircraft take-off mass, V_R is the aircraft rotational speed, n_{eng} is the number of jets, A_{jet} is the area of each jet at take-off and T_{jet} is the take-off jet temperature, taken to be constant. L/D is the aircraft lift to drag ratio during take-off and θ_{min} is the aircraft climb angle in degrees at the flyover position. The r.m.s. error between the prediction from this equation and the full optimization results was 0.34 dB. Noise modeling is discussed in §III.H.

$$N_{jet} = 45.75\log_{10}\left[mg\left(\frac{1}{L/D}+0.4\sin\theta_{\min}+0.05\right)\right]-39.94\log_{10}\left(\frac{n_{eng}A_{jet}}{T_{jet}}\right)+5.00\log_{10}\left(V_R\right)-254.5 \tag{2}$$

D. Engine Modeling

With high temperature jet noise reducing in proportion to approximately V^6 rather than V^8 as speed is reduced, avoiding a high temperature jet is critical. Therefore a fully mixed turbofan design was selected for the silent aircraft engine[3]. Thrust and jet exit parameters are dominated by fan capacity and performance, enabling the engine to be modeled as a fan with corrections to the exhaust flow that arises from bypass-core mixing. This approach is an extension of that in Ref 13 and is suitable as fan noise estimates can be made whilst at the same time ensuring the code is lightweight and suitable for take-off optimization. Equation (3) considers pressure rise from inlet to exhaust matching static pressure at the two conditions (after expansion the jet static pressure equals the free stream static pressure). Equation (4) looks at the net thrust produced by the engines, Eq. (5) covers nozzle choking and Eq. (6) matches fan and jet mass flows.

$$FPR = \frac{1}{PR_{in}PR_{out}}\left(\frac{1+\frac{\gamma-1}{2}M_{jet}^2}{1+\frac{\gamma-1}{2}M_\infty^2}\right)^{\frac{\gamma}{\gamma-1}} \tag{3}$$

$$\frac{T_N}{A_{jet}} = \gamma\, p_\infty M_{jet}^2\left(C_{FG}-\frac{M_\infty}{M_{jet}}\left(\frac{1+\frac{\gamma-1}{2}M_\infty^2}{1+\frac{\gamma-1}{2}M_{jet}^2}\right)^{-\frac{1}{2}}\left(FPR^{\frac{\gamma-1}{\gamma\eta_p}}+\frac{\Delta T_0}{T_{0\infty}}\right)^{-\frac{1}{2}}\right) \tag{4}$$

$$\frac{A_{noz}}{A_{jet}} = \max\left[1,M_{jet}\right]\left(\frac{2}{\gamma+1}\left(1+\frac{\gamma-1}{2}\max\left[1,M_{jet}\right]^2\right)\right)^{-\frac{1}{2}\left(\frac{\gamma+1}{\gamma-1}\right)} \tag{5}$$

$$\frac{A_{jet}}{A_{ff}} = \frac{\sqrt{FPR^{\frac{\gamma-1}{\gamma\eta_p}} + \Delta T_0/T_{0\infty}}}{FPR.PR_{out}} \frac{M_{ff}}{M_{jet}} \left(\frac{1+\frac{\gamma-1}{2}M_{ff}^2}{1+\frac{\gamma-1}{2}M_{jet}^2}\right)^{-\frac{1}{2}\left(\frac{\gamma+1}{\gamma-1}\right)} \qquad (6)$$

In these equations FPR is the mass averaged rise in stagnation pressure across the fan stage, PR_{in} is the pressure recovery (ratio of stagnation pressures) from free stream to the fan face and PR_{out} is the pressure recovery from fan stator exit to jet. PR_{in} includes any losses from ingested boundary layers and losses in the inlet ducting. PR_{out} includes losses in the exhaust duct and mixer along with any change in stagnation pressure of the bypass flow due to mixing with the core flow. C_{FG} is the thrust coefficient, close to one, and is defined here as the ratio of gross thrust delivered to the sum of the mass flow and jet velocity. ΔT_0 is the temperature rise of the bypass flow across the mixer due to mixing with the core.

For known aircraft parameters, Eqs. (1)-(6) enable sideline and flyover fan pressure ratio (FPR) to be calculated for a given jet noise target, N_{jet}. Top of climb FPR can then be calculated by specifying the design capacity and any change in nozzle area. For a low jet noise target, maintaining a fixed nozzle area leads to very low top of climb FPR and large fan face area, resulting in poor cruise performance and significant fan operability issues. In Ref 13 the change in nozzle area between take-off and top of climb / cruise was set so that cruise and flyover flow coefficients were matched (Eq. 7). This maximized fan efficiency at flyover and ensured the fan shock structure at sideline was ingested thus reducing rotor alone buzz-saw noise.

$$\varphi = \frac{V_x}{U} \propto \frac{M_{ff}\left(1+\frac{\gamma-1}{2}M_{ff}^2\right)^{-\frac{1}{2}}}{U} \qquad (7)$$

E. Operating with varying nozzle area

Opening the nozzle area at take-off leads to much improved fan operability but the start of roll stall margin is lower than that at flyover and, in some circumstances, the sideline fan efficiency can be poor. To resolve these issues the nozzle exit area can be continuously varied during take-off so that the fan is at all times working efficiently and away from stall, surge or flutter regions.

Achieving this requires a representative fan map, along with Eqs. (3)-(6), to be embedded into the take-off optimization routine. Rather than operating with a fixed nozzle area, it can instead be varied at each time-step so that the fan is operating at the ideal position for the required thrust. This is illustrated in Fig. 5. Top of climb FPR, which determines fan face area, is set to a level required for minimum fuel burn and during cruise the exit nozzle area can be set so as to operate at peak fan efficiency.

For a given thrust level at take-off, jet noise is minimized by operating with a large jet area and low jet velocity. This corresponds to moving down and to the right on the fan map as nozzle area is increased. The limit to this increase is set by two conditions: At low fan speed, negative incidence onto the fan outlet guide vanes is limiting and a static working line has been used to approximately track OGV incidence. At higher speed, fan choking is limiting as efficiency drops rapidly and fan operability issues occur when highly choked. For this limit the line $d\varphi/dM_{ff}=0$ can be used as the operating line up until maximum design capacity is achieved. This is because once choked the relative flow angle at fan face, which is the inverse tan of one over the flow coefficient, will remain fixed as back pressure is reduced further. This approach delivers low jet noise whilst ensuring fan operability and high efficiency at all times. As with Ref 13, blade speed can be set so that when the relative Mach number at the fan tip is greater than unity the primary shock structure is ingested.
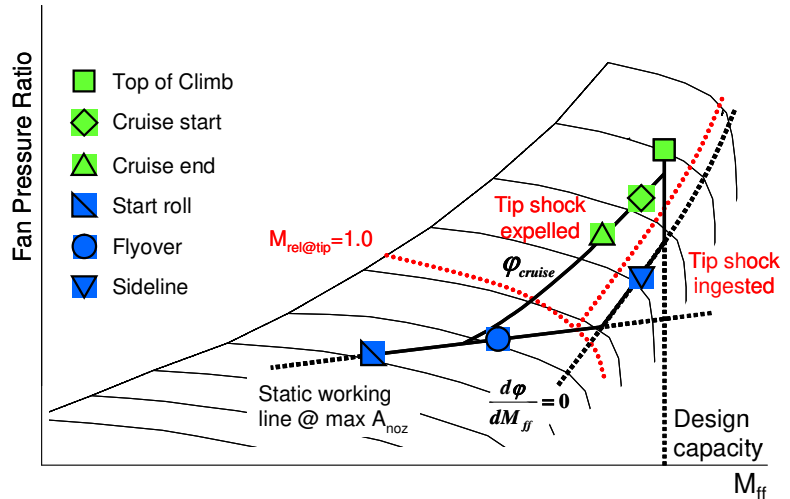

Figure 5. Fan operation with variable area nozzle for low take-off noise

F. Auxiliary Fans

The concept aircraft utilizes auxiliary fans driven by the primary engine in order to increase boundary layer ingestion, improve packaging and reduce fan source noise through increased fan blade passing frequency (BPF) and better liner attenuation. Each core drives three fans one of which is co-axial with the core with the other two offset and driven through a gearing arrangement[3]. While all fans have to operate at the same speed, for a fixed overall thrust the placement of the operating point along a line of constant speed is complicated as inlet and exit conditions are not necessarily matched. For simplicity the approach taken here is as follows:

- All fans are identical and operate at the same point of the fan map at all times.
- The core exhaust only mixes with the bypass flow from one of the fans. This is accounted for by the PR_{out} and ΔT_0 corrections.

This is achieved by having the nozzle area of each fan under separate control. The exhaust conditions of the fans are different and this is taken into account when calculating thrust and jet noise. Equations (3) to (6) are duplicated with versions existing for the core and the auxiliary fans. For the auxiliary version of the equations, ΔT_0 is zero and PR_{out} only accounts for duct losses.

The overall thrust requirement will be met by a combination of the thrust from the core and auxiliary fans as illustrated in Eq.(8) where n_{eng} is the total number of core fans and $n_{eng,aux}$ is the total number of auxiliary fans. This split can also be used when utilizing Eq.(2) with this more complicated engine arrangement. The total jet noise will be the sum of the noise from the core and auxiliary jets (Eq.(9) to Eq.(11)) with each supporting aircraft mass in proportion to their thrust.

$$T_{N,TOTAL} = n_{eng}T_N + n_{eng,aux}T_{N,aux}$$
$$\approx mg\left(\frac{1}{L/D}+\sin\theta\right) \tag{8}$$

$$N_{jet} = 45.75\log_{10}\left[\frac{n_{eng}T_N}{T_{N,TOTAL}}mg\left(\frac{1}{L/D}+0.4\sin\theta_{\min}+0.05\right)\right]-39.94\log_{10}\left(\frac{n_{eng}A_{jet}}{T_{jet}}\right)+5.00\log_{10}\left(V_R\right)-254.5 \tag{9}$$

$$N_{jet,aux} = 45.75\log_{10}\left[\frac{n_{eng,aux}T_{N,aux}}{T_{N,TOTAL}}mg\left(\frac{1}{L/D}+0.4\sin\theta_{\min}+0.05\right)\right]-39.94\log_{10}\left(\frac{n_{eng,aux}A_{jet,aux}}{T_{jet,aux}}\right)+5.00\log_{10}\left(V_R\right)-254.5 \tag{10}$$

$$N_{jet,TOTAL} = 10\log_{10}\left(10^{N_{jet}/10}+10^{N_{jet,aux}/10}\right) \tag{11}$$

G. Corrections for BLI and core mixing

Gasturb[23], a engine cycle design and analysis program, was used to estimate the corrections in exit pressure recovery and stagnation temperature that needed to be applied to account for bypass stream mixing with the engine core. Key operating points were specified and a simple relationship sought that could be utilized during the take-off optimization. The result of this work was the following two corrections that gave good agreement with GasTurb output. $PR_{out,ToC}$, $PR_{out,zero}$, $\Delta T_{0,ToC}$ and $\Delta T_{0,zero}$ are specified to match GasTurb output.

$$PR_{out} = PR_{out,zero}+\left(PR_{out,ToC}-PR_{out,zero}\right)\frac{FPR}{FPR_{ToC}}\frac{Q_{ff,ToC}}{Q_{ff}} \tag{12}$$

$$\Delta T_0 = \Delta T_{0,zero}+\left(\Delta T_{0,ToC}-\Delta T_{0,zero}\right)\frac{FPR-1}{FPR_{ToC}-1} \tag{13}$$

Boundary Layer Ingestion is used to increase cruise performance on the concept aircraft. Required thrust is reduced by ingesting and re-energizing the airframe suction surface boundary layer. This increases the specific fuel consumption but, if it can be supported by the engine, leads to an overall net benefit. From a preliminary analysis the impact on capacity was found to be significant but the impact on pressure rise and efficiency, small[4]. At take-off the ingested boundary layer relative to the streamtube capture area is much smaller than at cruise. To account for this the following three corrections were applied during take-off:

American Institute of Aeronautics and Astronautics

$$Q_{ff} = Q_{ff,no\_BLI}\left(1 - \Delta Q\frac{M_\infty}{M_{\infty,cruise}}\right) \tag{14}$$

$$PR_{in} = PR_{in,no\_BLI} - \Delta PR\frac{M_\infty}{M_{\infty,cruise}} \tag{15}$$

$$c_D = c_{D,no\_BLI} - \Delta c_D\frac{M_\infty}{M_{\infty,cruise}} \tag{16}$$

These corrections are approximate being based only on calculations at start of cruise and the observation that there is no boundary layer to ingest at zero flight speed. ΔQ is the percentage reduction in fan capacity at start of cruise due to BLI, ΔPR is the change in inlet pressure recovery at start of cruise due to BLI and Δc_D is the change in drag coefficient at start of cruise due to BLI. The corrected fan capacity is only used when calculating the mass flow rate (Eq.6) and is not used when estimating exit pressure recovery (Eq.12).

H. Noise Estimation

Initial analysis indicated that jet, fan and airframe noise were the dominant take-off noise sources and therefore rapid prediction of these values was required when optimizing the departure profile. The Stone noise model for a single jet was used to estimate jet mixing source noise[24] with no corrections applied to account for forced mixing between the core and bypass as the forced mixer is well upstream from the nozzle exit. Flight corrections from Low[25] were used rather than those internal to the Stone model as the work of Low covers jet to free stream velocities in the range used by the silent aircraft. If shock cell noise from under expanded jets was present, this was estimated using SAE ARP 876[26]. ARP 876 was not used for estimating jet mixing noise due to the large difference in prediction of flight correction effects when compared to the experimental work of Low.

Fan noise was estimated from ESDU correlations that cover broadband, tone and buzz-saw sources[27]. These correlations are based on the Heidmann model[28] with updated coefficients. Liners in the inlet and exhaust duct were used to attenuate the noise and the design of these liners along with calculations of their effectiveness can be found in Ref 29. Calculation of far-field noise when properly accounting for liner attenuation is computationally intensive and could not be integrated into the take-off optimization code. Instead, blanket corrections were applied to the source SPL values based on higher fidelity results at a few key points. Refraction, fourth power amplification and Doppler frequency shift corrections were then applied to the fan source noise hemispheres to account for flight effects. Finally, for forward propagating fan noise, shielding corrections were applied. These corrections, a function of polar angle, azimuthal angle and frequency, were based on low frequency estimations by Agarwal and Dowling[10] extended conservatively to higher frequencies.

Airframe noise emanates from the scattering of the boundary layer off of the airfoil trailing edge. This airfoil self-noise is the noise floor for a given configuration and is appropriate for analysis here because the aircraft uses a deployable drooped leading edge for lift augmentation, which has negligible direct noise emission[30], and the undercarriage will be stowed shortly after rotation. The airframe noise was estimated using empirical relationships based on the average chord and the area of the entire airframe in addition to global aircraft details such as approach velocity[31, 32].

When propagating the resultant source noise to the ground, atmospheric attenuation[33] and lateral attenuation[34] were accounted for and a +3dB correction made for ground reflection.

IV. Results

The results presented in this section are for the SAX40 concept aircraft described in detail elsewhere[2, 3]. Key airframe and engine parameters used as input to the take-off optimization can be found in Appendix B. The top of climb FPR for the concept aircraft was set to 1.50 based on results from earlier work with fan diameter fixed at 1.2m for each of the 9 fans (3 core and 6 auxiliary). With aircraft design iterations continuing beyond the setting of these values the final aircraft has an estimated 12.7% thrust margin at top of climb when climbing at 300ft/min (i.e. the engines can provide more thrust than is required). The results presented here are with the top of climb condition at maximum design thrust (i.e. FPR=1.50).

A. Trends with jet noise target

Before continuously varying the nozzle so as to operate as shown in Fig. 5, operation with a fixed nozzle area is briefly presented. Whilst this does not ensure the fan can deliver the required mass flow rate and pressure rise, it enables Eqs. (8)-(11) to be used rather than having to run full optimizations for each noise level under consideration.

Figure 6A is the result of this work showing the achievable fan pressure rise at different operating points for a given jet noise level at take-off. To create this figure the following approach was used: For a given ToC FPR and design fan capacity, the fan is sized for the required thrust level. Equation (1), which takes into account windmilling engine drag, can then be used to calculate the flyover climb angle to satisfy engine out safety requirements. Cruise capacity and pressure rise are then calculated with the cruise nozzle area matched to the top of climb nozzle area. Flyover FPR is set so that the cruise and flyover coefficients are matched (Eq.7). This requires the use of a representative fan map as flow coefficient is a function of blade speed and the fan map in Fig. 5 was used for this purpose. Matching flow coefficients fixes the take-off nozzle area enabling sideline conditions to be found and take-off jet noise estimated (Eqs. (8)-(11)). Data from appendix B was used without modification except for the temperature correction, ΔT_0, which was scaled with the fan pressure ratio minus one (to maintain an approximately constant ratio of bypass to core stagnation pressures into the mixer at the design point).
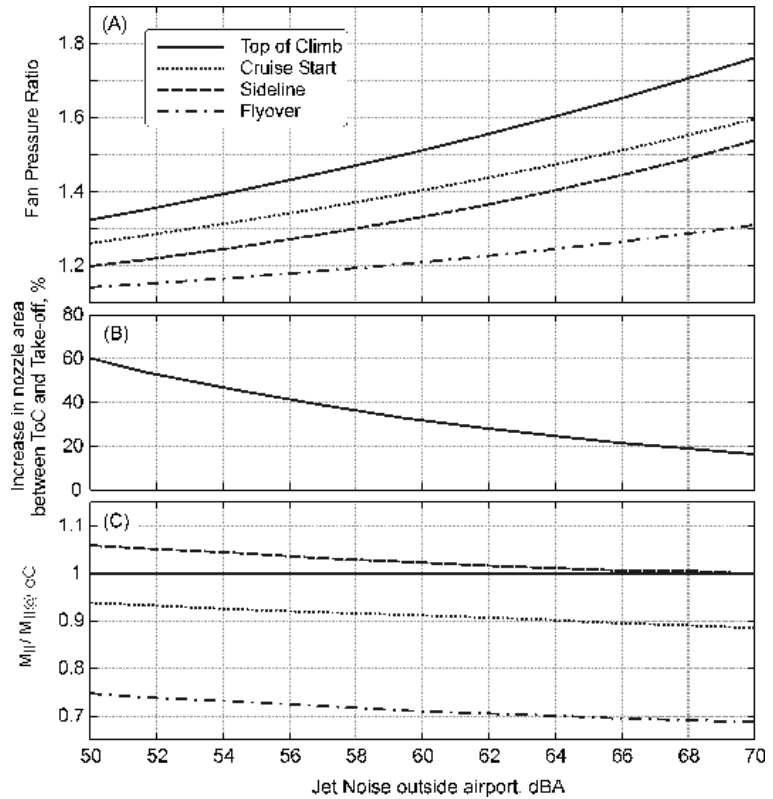

Figure 6. Variation in engine parameters with jet noise target

With the top of climb fan stage pressure ratio set at 1.50, Fig. 6A indicates that a jet noise level of approximately 59dBA should be achievable, below the overall noise target of 60dBA. To achieve this requires a nozzle area increase of approximately 35% between top of climb / cruise and take-off operation (Fig. 6B). As discussed in §III.E, operation with a fixed nozzle area at take-off can lead to the fan having to work at locations with poor performance or stability margin. For the SAX40 aircraft this is the case at sideline with the fan having to provide a pressure rise of 1.32 (Fig. 6A) at a fan face Mach number greater than the design capacity (Fig. 6C). This pressure rise is much less than the top of climb pressure rise and so the fan will be operating highly choked at sideline with poor efficiency and potential flutter problems. Therefore, although the results and trends outlined here are useful, full take-off optimization with the fan operating as prescribed in Fig. 5 is required to ensure the fan can deliver the required thrust at all times.

B. Optimization for minimum jet noise

With the engine operation integrated into the take-off optimization, Eqs. (8)-(11) are no longer used and instead at each time step the noise of each source is calculated on the ground around and beyond the airport boundary. Fan speed is reduced if the target is exceeded or increased if there is available margin with the nozzle area varied so as to stay on the prescribed fan operating line. Once the flyover point is passed the take-off is evaluated and then repeated with a modified noise target until all take-off requirements, and in particular the flyover climb angle, are satisfied.

Initially, with jet noise expected to be dominant, the take-off was optimized just for jet noise with the results shown in Fig. 7. From Fig. 6 it was estimated that a noise value of 59dBA would be achievable and, although that was for a fixed nozzle area and this is for a varying nozzle area, this noise level was approximately achieved (59.1 dBA was required to meet the flyover climb angle). In Fig. 7, the x-axis refers to the distance of the aircraft from brakes-off rather than the distance of the noise receiving location. The noise for each source is the estimate after liners, shielding and atmospheric effects have been taken into account. Further, the noise plotted is the maximum estimated for the source in question when the aircraft is at the specified location. With different directivity for each source the total aircraft noise shown is not the sum of the noise sources in the plot rather it is the sum of the noise sources at the maximum overall noise location.
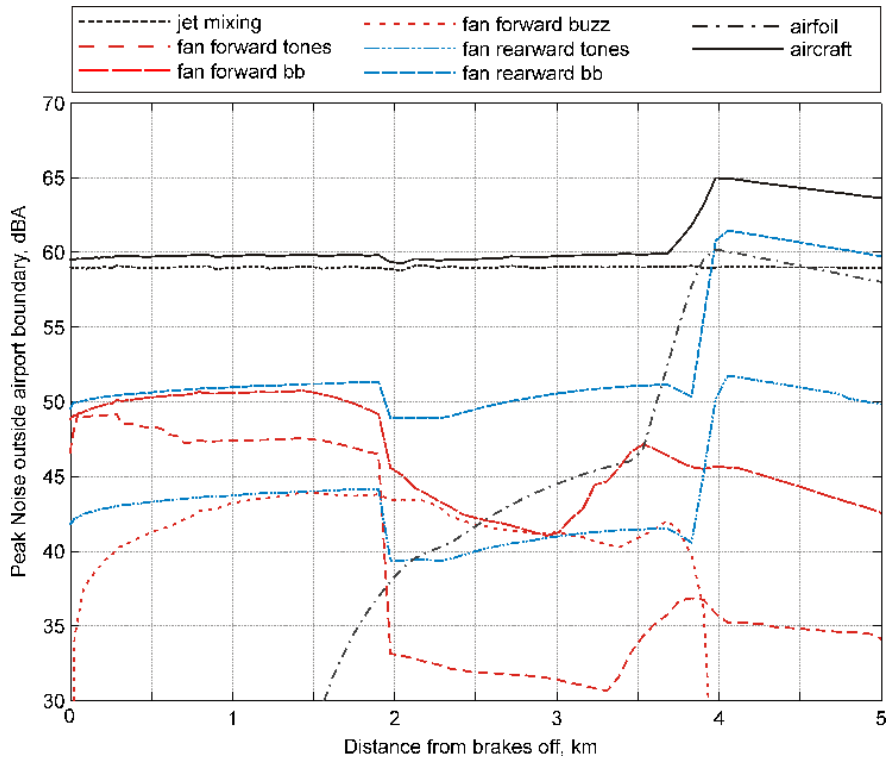
Figure 7. Estimated peak noise outside airport boundary when profile optimized for minimum jet noise.

Whilst jet noise is below the overall SAI noise target throughout the take-off, other noise sources become dominant at the flyover position giving an overall maximum noise level of 65dBA. This is because as the flyover position is approached the distance from aircraft to ground outside of the airport boundary drops rapidly from the square root of aircraft height and the sideline distance to just the aircraft height. With jet noise proportional to the eight power of velocity cutting back climb angle and thrust keeps jet noise at the required level. Fan noise sources scale with lower powers of velocity and therefore, relative to jet noise, increase. For the forward propagating fan noise this relative increase in noise is offset by the airframe shielding being much more effective when the receiver location is directly below the aircraft rather than along a sideline. For the rearward propagating fan noise there is no shielding and therefore significant noise increases on the ground are observed. Airframe noise, a function of aircraft velocity rather than engine operating condition, is not reduced by the cutback and so on-ground values increase rapidly. With the engines embedded into the airframe, shielding of forward propagating sources is much more effective that was initially envisaged leading to buzz-saw noise being 15dB below overall noise even when cut-on.

Figure 8 shows the operation of the fan during take-off both for low jet and low overall noise (see next section). When operating for low jet noise, the
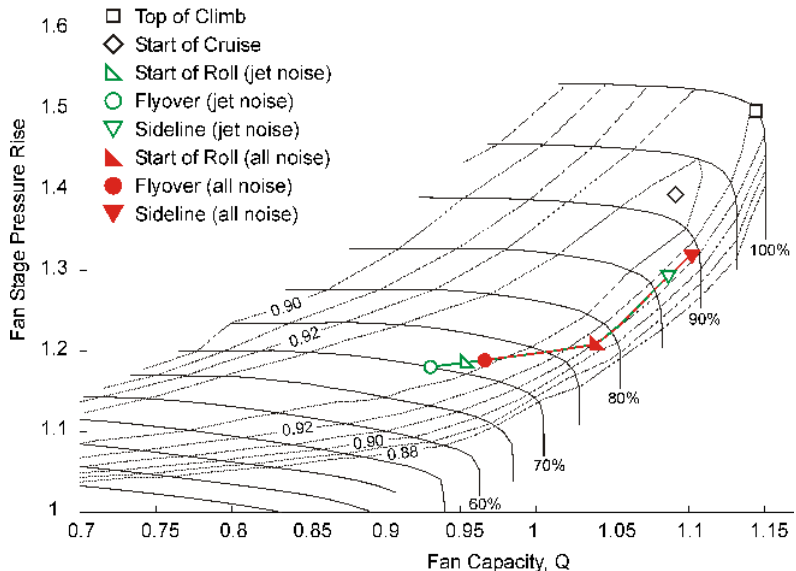

Figure 8. Fan operation during take-off when optimizing for just jet noise and for all noise sources. *Lines are constant fan corrected speed and contours are stage polytropic efficiency.*

American Institute of Aeronautics and Astronautics

start of roll position is at 72% fan speed with operation at high efficiency. This increases to 87% fan speed at sideline with nozzle area reduced to stop the fan operating at poor efficiency before cutting back to 70% at flyover. Figure 9 shows the variation in airframe and engine parameters in more detail from brakes off until 5km out, beyond the flyover location of 4048m. Take-off is approximately 2km after brakes off (subplot A) with climb angle rapidly increasing to 7.5° (subplot B). As height is gained lateral attenuation decreases and the climb angle has to reduce gradually to keep within the noise target. As the end of the airport boundary is approached the climb angle reduces rapidly to 2.85°, the minimum required to satisfy engine out safety conditions. Beyond the flyover point, with aircraft height continuing to increase, the climb angle can increase gradually.

With angle of attack increasing at the start of roll, aircraft L/D (subplot C) increases before reducing slightly as angle of attack increases beyond optimum. 50ft above ground the

Figure 9. Variation in aircraft and engine parameters during noise optimized take-off

undercarriage is stowed and L/D increases to approximately 23. With flight speed during take-off constant beyond this point (subplot D), angle of attack remains approximately constant and L/D remains at this level for the remainder of the noise constrained portion of the take-off. The rotational velocity of 65m/s leads to a climb speed of 75m/s. Looking at engine performance, the nozzle area is initially almost 60% greater than the top of climb value (subplot E) with overall net thrust of just over 250kN (subplot F). As sideline is approached the net thrust remains approximately constant with nozzle increase reduced to 30% as the fan moves up the operating line. Once climb starts, the thrust reduces to maintain a constant flight speed at reducing climb angle and this is accompanied by a gradual increase in nozzle area. At flyover the rapid reduction in thrust requires an increase in nozzle area to a value 45% higher than ToC. This is larger than the 35% nozzle increase expected from Fig. 6B and arises because the fan is operating slightly below and to the left of peak efficiency for the given thrust requirement (see Fig. 8). Finally it should be noted that whilst this departure satisfies accelerate-stop, field length and engine out requirements[18, 19] the main thrust cutback occurs approximately 50ft below the regulated cutback height of 800ft[35, 36].
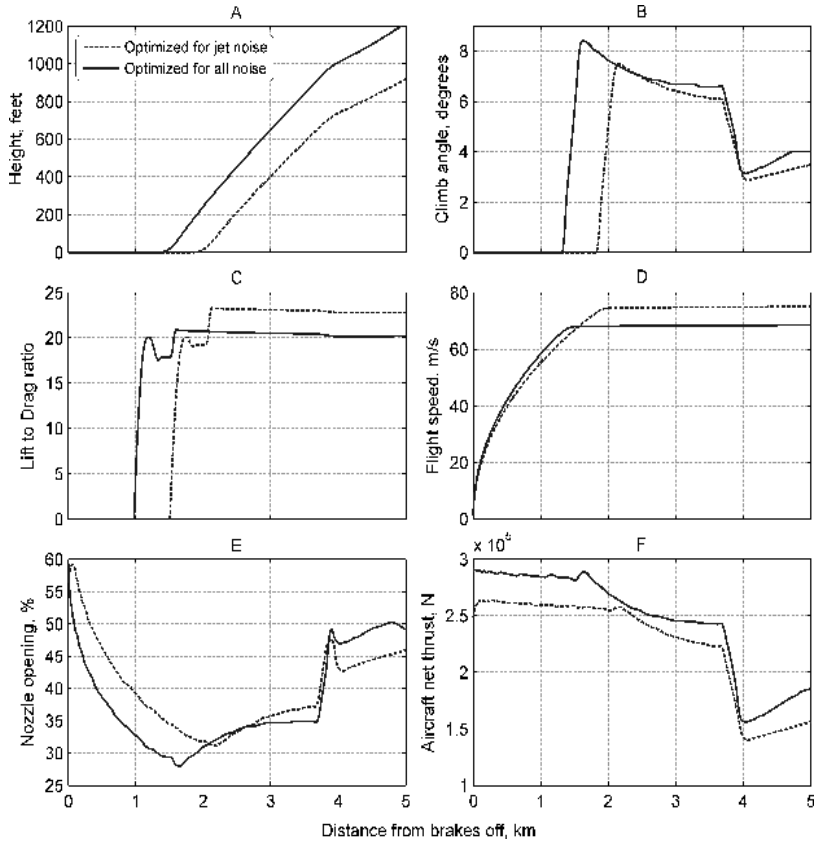
C. Optimization for minimum overall noise

To reduce the flyover noise level the take-off profile was optimized for all of the included noise sources; jet, fan and airframe. The resulting fan and aircraft operation are overlaid onto the results for jet noise only optimization in Fig. 8 and Fig. 9 respectively. With airframe noise insensitive to aircraft thrust and fan noise less sensitive than jet noise, the easiest way to reduce the overall flyover noise level is to increase the aircraft altitude at this point. This requires more rapid acceleration and earlier take-off as shown in Fig. 9 leading to increased start of roll and sideline noise. Roll velocity, V_R, is reduced from 65m/s to 57m/s which both enables earlier take-off and reduces airframe source noise. The downside of a reduced flight speed is an increase in the required angle of attack so as to maintain lift and a resulting reduction in the lift to drag ratio. The aircraft takes off approximately 500m earlier and is 1000ft rather than 750ft above the ground when cutback occurs, above the minimum regulated cutback height[35, 36]. Initial climb angle is just over eight degrees whilst the critical flyover climb angle is increased from 2.85° to 3.15°. This increase is required because the reduced L/D impacts the result of Eq.(1). With the aircraft accelerating quicker and climbing steeper the thrust provided by the engines is increased at all time steps. To maintain fan operation along the
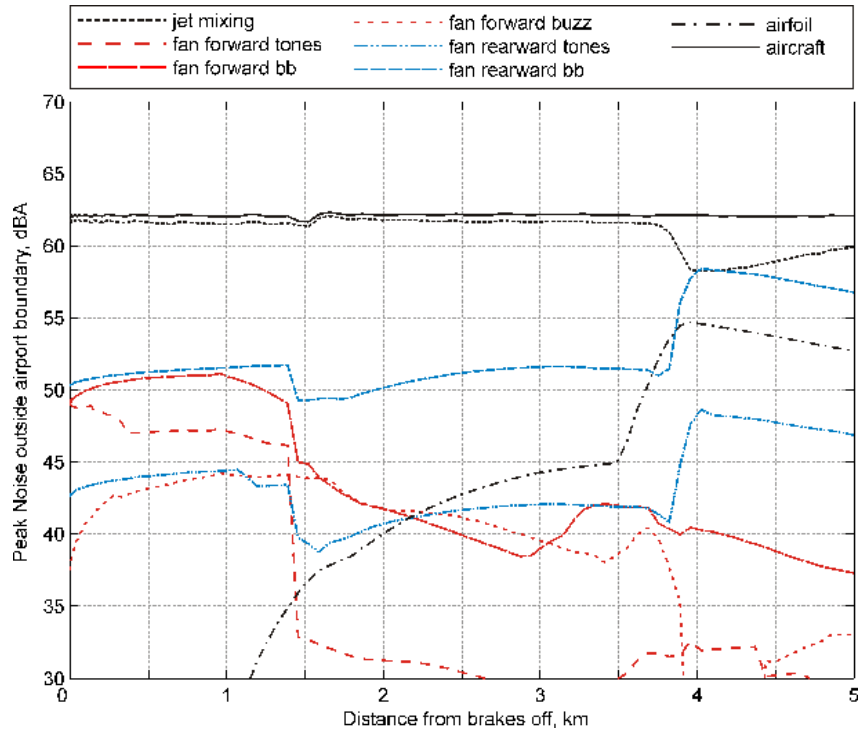
Figure 10. Estimated noise when profile optimized for minimum aircraft noise

prescribed working line this reduces the required increase in nozzle area. From Fig. 8 it can be seen that start of roll fan speed has been increased to 78%, sideline to almost 90% and flyover to 72%. The impact on fan efficiency at flyover is minimal with stage efficiency reducing from 93.4% to 93.2%.

Figure 10 shows the resulting peak noise outside of the airport boundary as the aircraft goes from brakes-off to 5km out. Overall, the start of roll and sideline noise levels have increases from 60dBA to 62dBA and the flyover noise level reduced from 65dBA to 62dBA. The reduced flight speed and increased aircraft height at flyover reduce airframe noise by 5dB and the increased height reduces fan rearward broadband noise by 3dB even with the slight thrust increase. Jet noise remains dominant at start of roll and sideline and is now also dominant along with fan rearward broadband noise at flyover.

D. Comparison with higher fidelity results at key locations

In the above results airframe shielding and liner attenuation predictions were relatively coarse. For shielding, low frequency results from Ref 10 were conservatively scaled to higher frequencies whilst for liner attenuation; blanket corrections to the source noise estimates were made. To validate these results alternative prediction of engine source noise levels were made for the take-off optimised for low overall noise at the key sideline and flyover locations. For sideline noise, the position was set at 2km after brakes off whilst for flyover noise the position was set at the airport boundary.
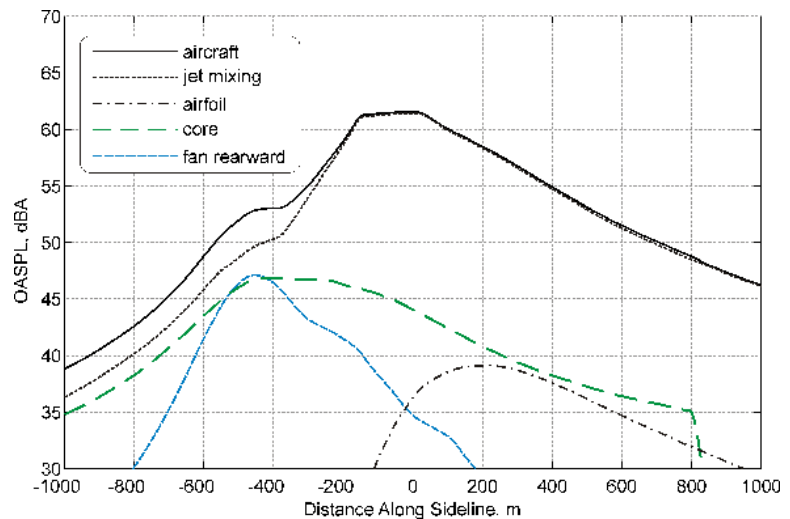

Figure 11. Estimated noise along sideline using higher fidelity modeling

American Institute of Aeronautics and Astronautics

Jet and airfoil modeling was unaffected with the approach discussed in §III.H followed but, instead of ESDU predictions, a version of Rolls Royce code was used in the estimation of engine source noise before liner attenuation and propagation. This code was also used in the prediction of core, turbine and compressor noise. Rearward propagating engine noise is modeled by solving appropriate eigenvalue problems for uniform axial inviscid flow in annular and cylindrical lined ducts. From the resulting modal amplitudes at the nozzle termination, the radiated sound pressure level is estimated using the Wiener-Hopf solutions from an unflanged duct[37, 38]. For forward noise sources shielding estimates are made by applying ray theory methods to the Silent Aircraft airframe geometry[39].
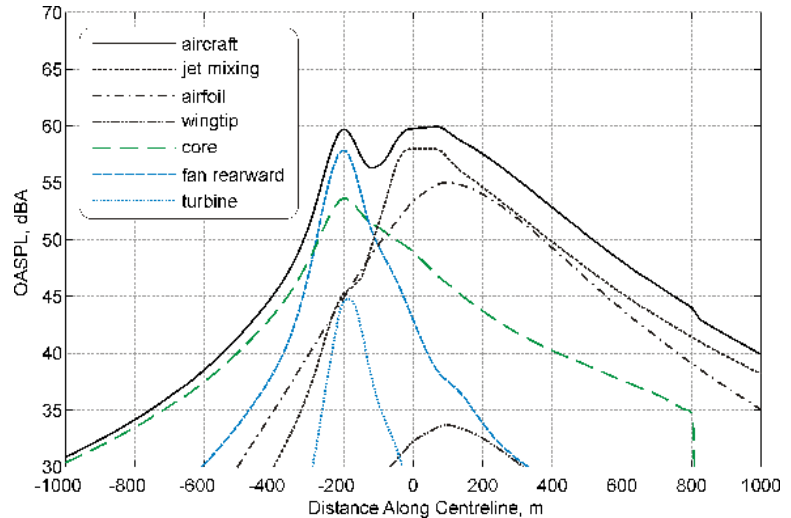

Figure 12. Estimated noise along centerline at flyover using higher fidelity modeling

Given a source distribution of forward propagating engine noise, it is assumed that in the shadow region, sound can only reach the observer through sharp edge diffraction or via creeping rays. The superposition of the resulting sound from the two mechanisms provides the noise beneath the aircraft. This approach provides an accurate way of quantifying the shielding effect but is too computationally intensive to be used during the take-off optimization.

Results are presented in Fig.11 for the sideline location and Fig.12 for the flyover location with the x-axis origin in both of these plots corresponding to the location of the aircraft. At the sideline location the same peak noise is estimated as would be expected with jet noise being dominant at this location. The same peak airframe noise also matches the earlier prediction but peak fan rearward noise is estimated to be 3dBA lower when using the approach described here than that presented above. Fan forward, turbine and compressor noise sources are all predicted to be minimal with extremely high reductions from airframe shielding and the turbine tones highly attenuated due to their very high frequency (see Ref 3 for details of the turbine design). At flyover the engine shaft speed reduction brings turbine noise into the audible range and a peak value of 45 dBA is estimated. Jet and airfoil peak noise match the peak levels expected from Fig. 10 and the same is true of the fan rearward noise. Overall noise is predicted to be 2dBA less than that given in Fig. 10 and, on investigation, this was found to be due to the fan rearward noise directivity: Whilst levels and directivity of the fan rearward source noise from the two models used are similar, differences occur once liner attenuation is accounted for. During the take-off optimization a blanket reduction was made to account for liners and this brings the estimated noise level down to that predicted in this subsection. This blanket correction was applied at all polar angles but, from the higher fidelity model, the liners are increasingly effective at greater polar angles relative to the jet exhaust. Therefore, as seen in Fig. 12, the peak fan noise level occurs a distance behind the aircraft and fan noise is highly attenuated ahead of this. (If the prediction of fan rearward noise from the previous section was overlaid onto Fig. 12, the peak level would be the same but it would extend forward to where jet and airfoil noise are also dominant.) This accounts for the 2dBA discrepancy in the overall noise prediction.

V. Discussion

This paper has presented the approach used and final result obtained when designing and operating for ultra low take-off noise as part of the Silent Aircraft Initiative. With the jet being a dominant noise source on take-off and the only way to significantly reduce jet noise being modification to the engine cycle, initial efforts focused on reducing jet noise to below the SAI target. This was achieved through introducing a variable area nozzle and optimizing the departure profile specifically for low jet noise. This approach proved successful with jet noise reduction to below the SAI target achieved even with a relatively high top of climb fan pressure ratio of 1.50.

Once the final design of the concept aircraft was complete it was possible to consider additional noise sources when optimizing the take-off profile including the fan and the airframe. These additional sources are only significant at flyover and, when optimizing for just jet noise, lead to flyover noise being approximately 5dBA above the SAI target. To minimize airframe and fan source noise requires the aircraft to be at increased altitude requiring additional

thrust earlier in the take-off. This leads to increased jet noise at the sideline location with an overall noise level of 62dBA being achieved throughout the take-off.

Apart from jet mixing noise, the dominant engine noise source is expected to be fan broadband rearward. Estimation of this noise source, which includes both rotor-stator interaction and rotor alone noise, is at the present time not as developed as the prediction of other noise sources. This is especially true when operating with a variable area nozzle as fan operating position at take-off is significantly different from conventional designs. This is discussed in more detail in Ref 13. Further, whilst boundary layer ingestion is much more significant at cruise than at take-off, there will still be some flow distortion onto the fan face during the noise critical period. This will impact forward and rearward propagating noise signatures but it is hard to know whether the overall peak fan noise on the ground will be increased as a result. Better understanding and prediction capabilities of fan rearward broadband noise are therefore required in order to increase the confidence of the overall SAI aircraft noise estimate.

With an overall noise signature estimated it is interesting to look at what changed could be made to future designs that might either reduce noise further or improve cruise fuel burn without impacting take-off noise. Firstly, shielding of forward propagating engine noise sources by the airframe was significantly more effective that initially envisaged. Future designs could possibly have reduced intake length to reduce weight without impacting the overall noise level. Similarly, the blade speed may not need to be set to control buzz-saw noise at flyover (as was discussed in more detail in Ref 13) although reducing it further and increasing the fan loading may reduce fan rearward noise. Making this decision requires a better understanding of how loading impacts noise when the fan rotor is operating near peak efficiency and well away from stall. Finally, reducing jet noise requires either a reduction in the design fan pressure ratio (and increase in engine size) or a reduction in the required thrust level. The current concept silent aircraft utilizes thrust vectoring in the vertical plane for pitch control. Extending this capability to the horizontal plane could replace the split aileron used for engine out yaw correction. This would minimize the L/D reduction on engine out reducing the critical flyover climb angle. This reduces the thrust required both at flyover and earlier in the take-off and will therefore enable a reduction in jet noise.

Finally, whilst the aim of the research and the optimization of the departure profile was to reduce noise as measured in dBA outside of the baseline airport boundary it is interesting to compare EPNdB values at the ICAO certification points with chapter four limits[40, 41]. For the aircraft departure profile optimised for low overall noise (Fig. 10) in which cutback is for the 4048m airport boundary noise estimates are 69.2 EPNdB at sideline and 68.8 EPNdB at the ICAO certification flyover distance of 6500m. When combined with the approach value of 71.4 EPNdB[5] this gives a cumulative noise of 209.4 EPNdB, 75dB below chapter four requirements.

Appendix A: Change in L/D following engine out

When the critical engine fails not only does the available thrust reduce but the overall drag also increases. In this appendix approximations of this drag increase are used to calculate the change in L/D following engine out during take-off for use in Eq.(1). With lift remaining approximately constant during engine out (L≈mg);
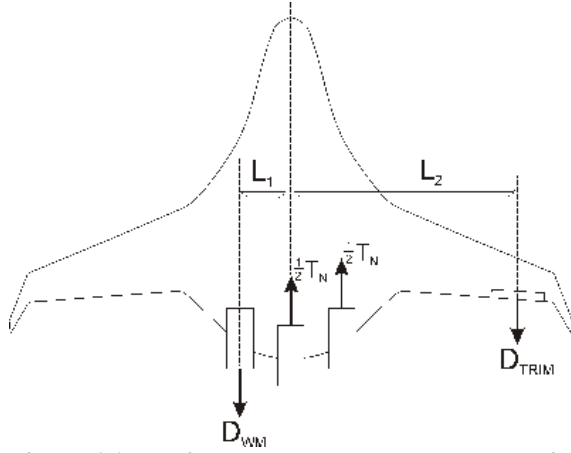

Figure A1: Engine out thrust and drag vectors in aircraft plane for 3 engine all-lifting-body configuration. *L_1 is the distance to the outboard (critical) engine, L2 the distance to the centre of drag for the split aileron.*

$$\frac{1}{L/D}\bigg|_{after} = \frac{1}{L/D}\bigg|_{before} + \frac{D_{wm} + D_{trim}}{L} \qquad \text{A.1}$$

where D_{wm} is the additional drag from the now windmilling engine (estimated using the approach of Kroo and Shevell[42], Eq.A2) and D_{trim} the additional control surface drag required to correct the resulting yaw.

$$D_{wm} \approx 0.0044 p_\infty A_{inlet} \approx 0.0044 p_\infty A_{ff} \qquad \text{A.2}$$

The control surface drag is a function of the remaining thrust which, for a small angle of attack can be estimated as;

$$T_N \approx D + D_{wm} + D_{trim} + mg\sin\theta^* \qquad \text{A.3}$$

where θ* is the climb angle after engine out and D is the drag before engine out. Figure A1 shows simplified force vectors for the all-lifting-body. With no tail the yaw correction must be achieved through alternative means and a split aileron (drag creation device) on the outer wing is used here:

$$D_{trim} \approx \frac{L_1}{L_2}\left(\frac{T_N}{n_{eng}-1} + D_{WM}\right) \approx \frac{D + n_{eng}D_{wm} + mg\sin\theta^*}{(n_{eng}-1)\frac{L_2}{L_1}-1} \qquad \text{A.4}$$

Appendix B: Concept Aircraft Parameters

Area	Parameter Name	Parameter Value
Aircraft	Take-off weight, m	150,822 kg
	Climb fuel	3,016 kg
	Cruise fuel	27,056 kg
	Wing Area	836 m^2
	Cruise Mach number	0.8
	Tire coefficient, μ	0.02
	Start of Cruise height	40,000 ft
	End of Cruise height	45,000 ft
	Rotation velocity, V_R	65m/s (optimizing for jet noise)
		57m/s (optimizing for all noise)
Engines	Number core engines	3
	Number auxiliary fans	6
	FPR at top of climb	1.50
	Design capacity, $Q_{ff,ToC}$	1.144 ($M_{ff,ToC} = 0.668$)
	ToC Excess Thrust (thrust margin when climbing at 300 ft/min at ToC conditions)	12.7%
	Thrust coefficient, C_{FG}	0.9935
	Liner correction, forward	5 dB
	Liner correction, buzz	10 dB
	Liner correction, rearward	22.5 dB
Atmospheric	ΔISA at take-off	12 K
	ΔISA at top of climb	10 K
	ΔISA at cruise	0 K
Corrections	$PR_{out,zero}$ (core engine exit PR at $M_\infty=0$)	0.9065
	$PR_{out,ToC}$ (core engine exit PR at $M_\infty=0.8$)	0.9457
	$PR_{out,aux}$ (auxiliary engine exit PR)	0.9800
	$\Delta T_{0,zero}$	33.3 K
	$\Delta T_{0,ToC}$	117.7 K
	ΔQ	4.2%
	PR_{in,no_BLI}	0.9898
	ΔPR (change in PR from BLI at cruise)	0.0343
	Δc_D (change in drag from BLI at cruise)	0.001372
Aircraft geometry for engine out calculation (appendix A)	L_1	7.3m
	L_2	26.4m
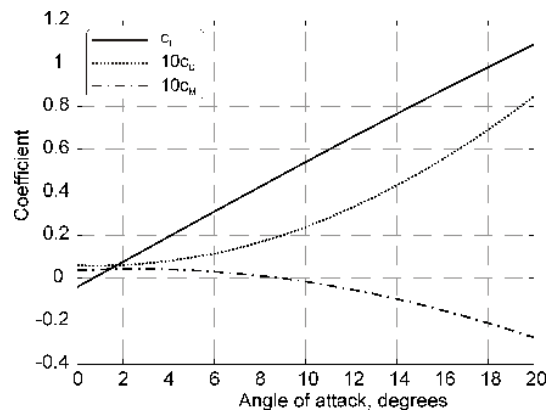
Figure B1. Airframe c_L, c_D and c_M at take-off (*c_M has nose down moment at high angle of attack*)

Acknowledgments

References

[1]Dowling, A. P., "The Silent Aircraft Initiative - Overview," *45th AIAA Aerospace Sciences Meeting and Exhibit*, AIAA-2007-0452. Reno, Nevada, 2007.

[2]Hileman, J. I., Spakovszky, Z. S., Drela, M., and Sargeant, M. A., "Airframe Design for 'Silent Aircraft'," *45th AIAA Aerospace Sciences Meeting and Exhibit*, AIAA-2007-0453. Reno, Nevada, 2007.

[3]de la Rosa Blanco, E., Hall, C. A., and Crichton, D., "Challenges in the Silent Aircraft Engine Design," *45th AIAA Aerospace Sciences Meeting and Exhibit*, AIAA-2007-0454. Reno, Nevada, 2007.

[4]Plas, A. P., Madani, V., Sargeant, M. A., Greitzer, E. M., Hall, C. A., and Hynes, T. P., "Performance of a Boundary Layer Ingesting (BLI) Propulsion System," *45th AIAA Aerospace Sciences Meeting and Exhibit*, AIAA-2007-0450. Reno, Nevada, 2007.

[5]Hileman, J. I., Reynolds, T.G., de la Rosa Blanco, E., and Law, T. R., "Development of Approach Procedures for the Silent Aircraft," *45th AIAA Aerospace Sciences Meeting and Exhibit*, AIAA-2007-0451. Reno, Nevada, 2007.

[6]Tam, R., Belobaba, P., Polenske, K. R., and Waitz, I., "Assessment of Silent Aircraft Enabled Regional Development and Economics in the UK," *45th AIAA Aerospace Sciences Meeting and Exhibit*, AIAA-2007-0455. Reno, Nevada, 2007.

[7]ACARE, "European Aeronautics: A vision for 2020," Advisory Council for Aeronautics Research in Europe, 2000.

[8]Berglund, B., Lindvall, T., and Schwela, D. H., "Guidelines for Community Noise," World Health Organization, 1999.

[9]Government, UK, "Noise Mapping England : The London Road Traffic Noise Map," Department for the Environment, Food and Rural Affairs (Defra), 2004.

[10]Agarwal, A. and Dowling, A. P., "Low Frequency Acoustic Shielding of Engine Noise by the Silent Aircraft Airframe," *11th AIAA/CEAS Aeroacoustics Conference*, AIAA 2005-2996. Monteray, California, 2005.

[11]Law, T. R. and Dowling, A. P., "Optimization of Traditional and Blown Liners for a Silent Aircraft," *12th AIAA/CEAS Aeroacoustics Conference*, AIAA-2006-2525. Cambridge, Massachusetts, 2006.

[12]Crichton, D., Tan, D, and Hall, C. A., "Required Jet Area for a silent aircraft at take-off," *8th ASC-CEAS Workshop* Budapest University of Technology and Economics, Hungary, 2004.

[13]Crichton, D., Xu, L, and Hall, C. A., "Preliminary fan design for a silent aircraft," *ASME Turbo Expo*, GT2006-90564. Barcelona, Spain, 2006.

[14]Hileman, J. I., Spakovszky, Z. S., Drela, M., and Sargeant, M. A., "Aerodynamic and Aeroacoustic Three-Dimensional Design for a 'Silent' Aircraft," *44th AIAA Aerospace Sciences Meeting and Exhibit*, AIAA-2006-0241. Reno, Nevada, 2006.

[15]Liebeck, R., "Design of the Blended Wing Body Subsonic Transport," *Journal of Aircraft*, Vol. 41, No. 1, 2004, pp. 10-25.

[16]Diedrich, A., Hileman, J., Tan, D., Willcox, K., and Spakovszky, Z. S., "Multidisciplinary Design and Optimization of the Silent Aircraft," *44th AIAA Aerospace Sciences Meeting and Exhibit*, AIAA-2006-1323. Reno, Nevada, 2006.

[17]Hall, C. A. and Crichton, D., "Engine Design Studies for a Silent Aircraft," *ASME Turbo Expo*, GT2006-90559. Barcelona, 2006.

[18]FAA, "Federal Aviation Regulations section 25: Airworthiness Standards: Transport Category Airplanes," Federal Aviation Administration.

[19]JAA, "Joint Aviation Regulations section 25: Airworthiness Standards: Transport Category Airplanes," Joint Aviation Administration.

[20]ICAO, "Convention on International Civil Aviation - Annexe 16, Volume 1, Third Edition," 1993.

[21]MetOffice, "Land Surface Observation Stations Data," British Atmospheric Data Centre.

[22]Crichton, D., "Fan Design and Operation for Ultra Low Noise," Ph.D. Dissertation, Department of Engineering, University of Cambridge, Cambridge, England, 2007 (to be published).

[23]Kurzke, J., "GasTurb." 2004. p. Gas Turbine Cycle Analysis Programme.

[24]Stone, J. R., Groesbeck, D. E., and Zola, C. L., "Conventional Profile Coaxial Jet Noise Prediction," *AIAA Journal*, Vol. 21, No. 3, 1983, pp. 336-342.

[25]Low, J.K.C., "Ultra-High Bypass Ratio Jet Noise," NASA CR-195394, 1994.

[26]SAE, "Gas Turbine Jet Exhaust Noise Prediction," ARP876 revision D, 1994.

[27]ESDU, "Prediction of noise generated by fans and compressors in turbojet and turbofan engines," Item 98008, 1998.

[28]Heidmann, M. F., "Interim Prediction Method for Fan and Compressor Source Noises," NASA TM X-71763, 1979.

[29]Law, T. R. and Dowling, A. P., "Optimisation of Annular and Cylindrical Liners for Mixed Exhaust Aeroengines," *13th AIAA/CEAS Aeroacoustics Conference* Rome, Italy, 2007 (to be published).

[30]Andreou, C., Graham, W., and Shin, H-C., "Aeroacoustic Study of Airfoil Leading Edge High-Lift Devices," *12th AIAA/CEAS Aeroacoustics Conference*, AIAA-2006-2515. Cambridge, Massachusetts, 2006.

[31]Fink, M. R., "Airframe Noise Prediction Method," FAA-RD-77-29 (available from DTIC as AD A039 664), 1977.

[32]ESDU, "Airframe Noise Prediction," Item 90023 Amendment C, 2003.

[33]ESDU, "Evaluation of the Attenuation of Sound by a Uniform Atmosphere," Item 78002, 1977.

[34]ESDU, "Estimation of Lateral Attenuation of Air-to-Ground Jet or Turbofan Aircraft Noise in one-third octave bands," Item 82027, 1982.

[35]ICAO, "PANS-OPS Volume 1 Part V : Noise Abatement Procedures," International Civil Aviation Organization.

[36]FAA, "Noise Abatement Departure Profiles," AC 91-53A, Federal Aviation Administration, 1993.

[37]Munt, R. M., "The Interaction of Sound with a Subsonic Jet Issuing from a Semi Infinite Cylindrical Pipe," *Journal of Fluid Mechanics*, Vol. 83, 1977, pp. 609-640.

[38]Gabard, G. and Astley, R. J., "Theoretical Model for Sound Radiation from Annular Jet Pipes: Farfield and Nearfield Predictions," *Journal of Fluid Mechanics*, Vol. 549, 2006, pp. 315-341.

[39]Agarwal, A., Dowling, A. P., Shin, H-C., Graham, W., and Sefi, S., "A Ray Tracing Approach to Calculate Acoustic Shielding by the Silent Aircraft Airframe," *12th AIAA/CEAS Aeroacoustics Conference*, AIAA-2006-2618. Cambridge, Massachusetts, 2006.

[40]FAA, "Federal Aviation Regulations section 36: Noise Standards: Aircraft Type and Airworthiness Certification," Federal Aviation Association.

[41]JAA, "Joint Aviation Regulations section 36: Noise Standards: Aircraft Type and Airworthiness Certification," Joint Aviation Association.

[42]Kroo, I. M. and Shevell, R. S., "Aircraft Design: Synthesis and Analysis," Desktop Aeronautics Inc., 2006.